Frequency response of periodically sheared homogeneous turbulence

Peter E. Hamlington[a] and Werner J. A. Dahm
Department of Aerospace Engineering, Laboratory for Turbulence and Combustion (LTC), The University of Michigan, Ann Arbor, Michigan 48109-2140, USA

(Received 18 August 2008; accepted 13 April 2009; published online 28 May 2009)

A detailed parametric study is presented for the dynamics of initially isotropic homogeneous turbulence subjected to periodic shear with magnitude S and frequency ω. The study is based on a quasianalytical solution to the anisotropy transport equation, which is shown to provide results for the shear anisotropy in this flow that agree well with direct numerical simulation (DNS), and for some key aspects of the dynamics agree better than do the most widely used second-order moment closures. The present analytical approach allows a more detailed parametric study than is practical via DNS, and provides direct insights into the parametric origins of the resulting dynamics. The long-time limit form of the shear anisotropy provides an analytical expression for the phase lag. The general solution also provides simple scalings in the full equilibrium limit as well as in the quasiequilibrium and saturated nonequilibrium regimes. The transition to the saturated nonequilibrium regime is shown to occur over a narrow range of ω around a critical frequency ω_{cr}, for which an analytical expression is also obtained. The fundamental change in the dynamics of the turbulence kinetic energy $k(t)$ and the turbulence relaxation time scale $\Lambda(t)$ as ω increases beyond ω_{cr} is additionally addressed. © *2009 American Institute of Physics*. [DOI: 10.1063/1.3140003]

I. INTRODUCTION

The frequency response of initially isotropic homogeneous turbulence subjected to a periodic strain field $\bar{S}_{ij}(t)$ is fundamentally important, in part to understand effects of unsteady forcing on turbulent flows, but even more so for understanding anisotropy in steady inhomogeneous turbulent flows. In the latter, Lagrangian time variations,

$$\frac{D\bar{S}_{ij}}{Dt} = \left[\frac{\partial}{\partial t} + \bar{u}_l \frac{\partial}{\partial x_l}\right]\bar{S}_{ij}, \tag{1}$$

of the mean strain arise due to spatial gradients in the mean flow. The turbulence is then subjected to time variations in the mean strain as it moves along the mean flow streamlines. While there are additional effects of spatial inhomogeneities on the resulting turbulence anisotropy, which are not present in the homogeneous periodically sheared case considered here, this relatively simple flow nevertheless gives important insights into nonequilibrium effects on turbulence anisotropy due to changes in the mean strain.

In initially isotropic periodically sheared turbulence,[1] the mean strain rate tensor $\bar{S}_{ij}(t)$, given by

$$\bar{S}_{ij} \equiv \frac{1}{2}\left(\frac{\partial \bar{u}_i}{\partial x_j} + \frac{\partial \bar{u}_j}{\partial x_i}\right), \tag{2}$$

is zero for $t<0$ and for $t\geq 0$ varies in time according to

$$\bar{S}_{12}(t) = \bar{S}_{21}(t) = (S/2)\sin(\omega t), \tag{3}$$

where S is the amplitude and ω is the shearing frequency, and where all other components of $\bar{S}_{ij}$ are zero. For sufficiently large ω, the time scale on which the shear varies can become much faster than the turbulence response time scale, leading to substantial nonequilibrium between the turbulence and the applied shear. Such "nonequilibrium turbulence" gives rise to frequency-dependent anisotropy that the most widely used turbulence models based on the classical Boussinesq hypothesis—which are typically intended only for the equilibrium limit—cannot account for.

Investigations into the effects of unsteady forcing of turbulence have included direct numerical simulations (DNS), large eddy simulations, and second-order moment closures of the Reynolds-averaged Navier–Stokes (RANS) equations. Rapid distortion theory (RDT) has also been used to investigate nonequilibrium effects, such as in homogeneous turbulence subjected to rotating shear.[2] However, for periodically sheared homogeneous turbulence as in Eq. (3), RDT cannot be used[1] due both to the reversibility properties of the RDT equations and the invalidity of the linearized Navier–Stokes equations when the applied mean strain $\bar{S}_{ij}(t)$ is near zero. In a related problem, the response of isotropic turbulence to periodic forcing has been studied using mean-field[3,4] and spectral closure[5] approaches. Here, however, we seek to understand the anisotropy and nonequilibrium effects that result in turbulence from unsteadiness in the applied mean strain $\bar{S}_{ij}$. In particular, our goal is to better understand how the anisotropy dynamics in periodically sheared homogeneous turbulence depend on the shearing frequency ω and amplitude S.

A recent DNS study by Yu and Girimaji[1] of initially isotropic homogeneous turbulence subjected to periodic shear has revealed some aspects of the frequency response produced by unsteady shearing of turbulent flows. In particular, the DNS results show a frequency-dependent phase lag

[a]Author to whom correspondence should be addressed. Electronic mail: peterha@umich.edu.

 © 2009 American Institute of Physics

Downloaded 29 May 2009 to 141.24.81.5. Redistribution subject to AIP license or copyright; see http://pof.aip.org/pof/copyright.jsp

between the applied shear $\bar{S}_{12}(t)$ and the resulting Reynolds shear stress anisotropy $a_{12}(t)$, with a_{ij} defined as

$$a_{ij} \equiv \frac{\overline{u_i' u_j'}}{k} - \frac{2}{3}\delta_{ij}, \tag{4}$$

where $\overline{u_i' u_j'}$ is the Reynolds stress tensor and $k \equiv \frac{1}{2}\overline{u_i' u_i'}$ is the turbulence kinetic energy. The DNS results have also revealed a transition from asymptotic growth in $k(t)$ at low shearing frequencies to asymptotic decay above a critical frequency $\omega_{cr} \approx 0.5S$. Somewhat similar frequency-dependent nonequilibrium features have also been observed in turbulence subjected to time-varying plane strain.[6,7]

While the computational burden of DNS necessarily limits the extent of any detailed parametric study of periodically sheared turbulence dynamics, accurate second-order RANS closures could, in principle, allow a more extensive parametric investigation. In general, however, accurate prediction of nonequilibrium dynamics in the anisotropy and energetics of turbulence poses a significant challenge for turbulence modeling. The widely used Launder, Reece, and Rodi (LRR) model[8] and Speziale, Sarkar, and Gatski (SSG) model,[9] for example, were found[1] to significantly underpredict the critical shearing frequency ω_{cr} observed in the DNS study of Yu and Girimaji. The most widely used closures based on the Boussinesq hypothesis are completely incapable of accurately producing the nonequilibrium anisotropy dynamics in periodically sheared homogeneous turbulence.[1,10]

Here we extend the earlier DNS study of Yu and Girimaji[1] to present a relatively complete parametric analysis for the frequency response of periodically sheared homogeneous turbulence, using a new nonequilibrium closure developed in Ref. 10. A quasilinear form of the complete dynamical equation for the anisotropy $a_{ij}(t)$ is used to obtain an approximate quasianalytical solution for the anisotropy under the effect of periodic shear. The resulting solution shows good agreement with DNS, and correctly gives the frequency-dependent amplitude and phase lag between the anisotropy and the applied shear over the entire range of frequencies, from the full equilibrium limit through the saturated nonequilibrium regime. It also provides an analytical result for the critical shearing frequency ω_{cr}. This approach furthermore gives analytical scalings for key dynamical quantities such as the anisotropy, the production-to-dissipation ratio, and the turbulence time scale in the full equilibrium limit as well as the quasiequilibrium and saturated nonequilibrium regimes. The simplicity of this approach, combined with its accuracy in reproducing results from DNS, thus permits a detailed parametric frequency response analysis of periodically sheared homogeneous turbulence.

The paper is organized as follows. In Sec. II the approximate solution for the anisotropy in periodically sheared turbulence is derived from the anisotropy transport equation. The time evolution of the anisotropy is compared with results from second-moment RANS models and DNS, and the frequency dependence of the phase lag and anisotropy amplitude are then examined analytically using the present model in the full equilibrium and saturated nonequilibrium limits. In Sec. III the time evolution and frequency response of the turbulence kinetic energy production-to-dissipation ratio are considered, while Sec. IV presents results for the turbulence kinetic energy and relaxation time. Conclusions are presented in Sec. V.

II. APPROXIMATE SOLUTION FOR PERIODICALLY SHEARED TURBULENCE

In this section, an approximate analytical solution for the anisotropy $a_{ij}(t)$ in periodically sheared homogeneous turbulence is developed from the anisotropy transport equation.

A. Anisotropy transport equation

From the definition of the anisotropy in Eq. (4) and the general form of the Reynolds stress transport equation,[11] the exact dynamical equation for $a_{ij}(t)$ can be written as[9,12]

$$\frac{Da_{ij}}{Dt} = -\left(\frac{P}{\epsilon} - 1\right)\frac{\epsilon}{k}a_{ij} + \frac{1}{k}\left[P_{ij} - \frac{2}{3}P\delta_{ij}\right] + \frac{1}{k}\Pi_{ij} + \frac{1}{k}\left[D_{ij} - \left(a_{ij} + \frac{2}{3}\delta_{ij}\right)D\right]. \tag{5}$$

Here D/Dt is the mean flow Lagrangian derivative, ϵ is the dissipation rate of the turbulence kinetic energy k, $P_{ij} \equiv -\overline{u_i' u_l'}(\partial \bar{u}_j/\partial x_l) - \overline{u_j' u_l'}(\partial \bar{u}_i/\partial x_l)$ is the corresponding production tensor, where $P \equiv P_{ll}/2$ is the kinetic energy production rate, Π_{ij} is the pressure-strain correlation tensor, D_{ij} is the combined viscous and turbulent transport tensor, where $D \equiv D_{ll}/2$, and isotropy has been assumed for the dissipation rate tensor so that $\epsilon_{ij} = \frac{2}{3}\epsilon\delta_{ij}$. In homogeneous turbulent flows both D_{ij} and D are exactly zero.

The pressure-strain correlation Π_{ij} can be expanded[9,12] in terms of a_{ij} as

$$\Pi_{ij} = -C_1\epsilon a_{ij} + C_2 k\bar{S}_{ij} + C_3 k\left(a_{il}\bar{S}_{lj} + \bar{S}_{il}a_{lj} - \tfrac{2}{3}a_{nl}\bar{S}_{nl}\delta_{ij}\right) - C_4 k(a_{il}\bar{W}_{lj} - \bar{W}_{il}a_{lj}) + C_5\epsilon\left(a_{il}a_{lj} - \tfrac{1}{3}a_{nl}a_{nl}\delta_{ij}\right), \tag{6}$$

where

$$\bar{W}_{ij} \equiv \frac{1}{2}\left(\frac{\partial \bar{u}_i}{\partial x_j} - \frac{\partial \bar{u}_j}{\partial x_i}\right) \tag{7}$$

and the C_i are constants that may depend on invariants of a_{ij}. Using the form for Π_{ij} in Eq. (6) and writing P_{ij} in terms of a_{ij}, $\bar{S}_{ij}$, and $\bar{W}_{ij}$, the resulting dynamical equation for the anisotropy tensor a_{ij} in homogeneous turbulence is

$$\frac{da_{ij}}{dt} = -\alpha_1\frac{\epsilon}{k}a_{ij} + \alpha_2\bar{S}_{ij} + \alpha_3\left(a_{il}\bar{S}_{lj} + \bar{S}_{il}a_{lj} - \frac{2}{3}a_{nl}\bar{S}_{nl}\delta_{ij}\right) - \alpha_4(a_{il}\bar{W}_{lj} - \bar{W}_{il}a_{lj}) + \alpha_5\frac{\epsilon}{k}\left(a_{il}a_{lj} - \frac{1}{3}a_{nl}a_{nl}\delta_{ij}\right), \tag{8}$$

where the α_i coefficients are

Downloaded 29 May 2009 to 141.24.81.5. Redistribution subject to AIP license or copyright; see http://pof.aip.org/pof/copyright.jsp

$$\alpha_1 = \left(\frac{P}{\epsilon} - 1 + C_1\right), \quad \alpha_2 = \left(C_2 - \frac{4}{3}\right), \quad \alpha_3 = (C_3 - 1),$$
$$\alpha_4 = (C_4 - 1), \quad \alpha_5 = C_5. \tag{9}$$

For the most common second-order RANS closures, the constants C_i are taken as

$$C_1 = 1.5, \quad C_2 = 0.8, \quad C_3 = 0.875, \quad C_4 = 0.655, \quad C_5 = 0, \tag{10}$$

in the LRR model,[8] and as

$$C_1 = 1.7 + 0.9\frac{P}{\epsilon}, \quad C_2 = 0.8 - 0.65(II_a)^{1/2},$$
$$C_3 = 0.625, \quad C_4 = 0.2, \quad C_5 = 1.05, \tag{11}$$

in the SSG model,[9] where $II_a \equiv a_{nl}a_{ln}$ is the second invariant of the anisotropy tensor.

B. Quasilinear anisotropy dynamics

In contrast to such second-order RANS closures, where the full set of six coupled differential equations in Eq. (8) must be integrated, here we obtain an approximate quasi-analytical solution for periodically sheared homogeneous turbulence by retaining only the leading terms in Eq. (8). It has been noted[13] that the quadratic α_5 term in Eq. (8) is typically small, and it is common to set $C_5=0$ as in Eq. (10). Moreover, it will be seen herein that the contribution from the α_3 and α_4 terms to the anisotropy dynamics in periodically sheared turbulence is substantially less than that from the leading α_2 term. Taking the α_3, α_4, and α_5 terms in Eq. (8) together to be negligible thus gives an approximate quasilinear dynamical equation[10] for the anisotropy $a_{ij}(t)$ as

$$\frac{da_{ij}}{dt} = -\frac{1}{\Lambda}a_{ij} + \alpha_2\bar{S}_{ij}, \tag{12}$$

where

$$\Lambda \equiv \frac{1}{\alpha_1}\frac{k}{\epsilon} \tag{13}$$

is the turbulence relaxation time scale. Despite neglect of the higher-order terms, Eq. (12) still contains the primary nonequilibrium (da_{ij}/dt), relaxation ($-a_{ij}/\Lambda$), and rapid strain ($\alpha_2\bar{S}_{ij}$) dynamics governing the evolution of the anisotropy for periodically sheared turbulence. Figure 1 shows for $\omega/S=0.5$ that the evolution of a_{12} predicted by Eq. (12) is in good agreement with results from the full a_{ij} equation in Eq. (8) using the constants in Eq. (10), with only slight amplitude discrepancies at the maxima and minima of each cycle. Physical justification for Eq. (12) has been outlined in Ref. 10, and it will be seen herein that for periodically sheared homogeneous turbulence the terms excluded in Eq. (12) are not essential to obtain good agreement of the turbulence dynamics with corresponding DNS results.

The quasilinear dynamical equation in Eq. (12) has an exact solution[10] of the form

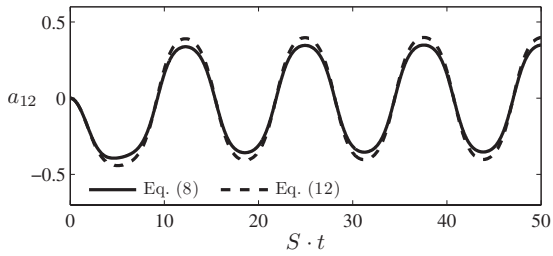

FIG. 1. Comparison of anisotropy $a_{12}(t)$ from full a_{ij} equation in Eq. (8) and truncated form in Eq. (12) for shearing frequency $\omega/S=0.5$; both curves are for constants in Eq. (10).

$$a_{ij}(t) = \int_{-\infty}^{t} \alpha_2\bar{S}_{ij}(\tau)h(t-\tau)d\tau, \tag{14}$$

where $a_{ij}(-\infty) \equiv 0$ and the impulse response function is given by

$$h(t-\tau) \equiv \exp\left[-\int_{\tau}^{t}[\Lambda(t')]^{-1}dt'\right]. \tag{15}$$

In Eqs. (14) and (15), the entire time history of both the applied mean shear $\bar{S}_{ij}(t)$ and the turbulence relaxation time scale $\Lambda(t)$ are reflected in the resulting $a_{ij}(t)$. Expanding the inverse of the relaxation time scale $\Lambda(t')$ around the current time t and integrating, Eq. (15) can be written as

$$h(t-\tau) = \exp\left[-\frac{(t-\tau)}{\Lambda(t)} + \frac{1}{2}(t-\tau)^2\frac{d(1/\Lambda)}{dt} + \cdots\right]. \tag{16}$$

Here it is assumed that the derivative terms in Eq. (16) are negligible relative to the leading term, thus ignoring the explicit time history of Λ in the a_{ij} dynamics. However, the history of Λ in Eq. (13) is still accounted for indirectly through the dynamical equations for k and ϵ presented in the next section, and it will be seen in the following that the neglected terms in Eq. (16) are not essential for accurately capturing the anisotropy dynamics in periodically sheared turbulence. With this approximation, the anisotropy in Eq. (14) is then given as

$$a_{ij}(t) = \int_{-\infty}^{t} \alpha_2\bar{S}_{ij}(\tau)e^{-(t-\tau)/\Lambda(t)}d\tau. \tag{17}$$

The fixed point ($da_{ij}/dt=0$) solution to Eqs. (12) and (13), as well as the solution to Eq. (17) for constant $\bar{S}_{ij}(t)$, recovers the classical Boussinesq equilibrium anisotropy closure

$$a_{ij} = -2C_\mu\frac{k}{\epsilon}\bar{S}_{ij}, \tag{18}$$

where the coefficient C_μ found in many linear eddy viscosity models is defined as

$$C_\mu \equiv -\frac{\alpha_2}{2\alpha_1}. \tag{19}$$

The convolution integral in Eq. (17) can thus be written as

Downloaded 29 May 2009 to 141.24.81.5. Redistribution subject to AIP license or copyright; see http://pof.aip.org/pof/copyright.jsp

$$a_{ij}(t) = -2C_\mu \alpha_1 \int_{-\infty}^{t} \bar{S}_{ij}(\tau) e^{-(t-\tau)/\Lambda(t)} d\tau. \tag{20}$$

The form in Eq. (20) is the nonequilibrium anisotropy closure in Ref. 10, where it has been examined in a variety of nonequilibrium test cases, and for later comparison with the LRR and SSG models is herein denoted the HD model. Taking the standard value

$$C_\mu \approx 0.09 \tag{21}$$

and using the equilibrium value $P/\epsilon \approx 1.89$ in Eq. (9), the constants in Eq. (10) give $\alpha_1 = 2.39$ for the LRR model, and in Eq. (11) give $\alpha_1 = 4.29$ for the SSG model. It will be seen herein that for the HD model in Eq. (20) the value

$$\alpha_1 = 3.57 \tag{22}$$

gives good agreement for periodically sheared homogeneous turbulence with the DNS results of Yu and Girimaji.[1]

C. Solution for periodically sheared turbulence

Unlike the LRR and SSG models, the HD model in Eq. (20) for the periodic shear in Eq. (3) gives an analytical solution for the resulting shear anisotropy $a_{12}(t)$ as

$$a_{12}(t) = -C_\mu \alpha_1 \left(\frac{S}{\omega}\right)\left[\frac{\omega\Lambda}{1+(\omega\Lambda)^2}\right] \times \{\sin(\omega t) - (\omega\Lambda)[\cos(\omega t) - e^{-t/\Lambda}]\}. \tag{23}$$

The anisotropy in Eq. (23) can be seen to vary at the same frequency ω as the applied shear, while the amplitude, phase, and initial transient from the $e^{-t/\Lambda}$ term all depend on the nondimensional parameter $(\omega\Lambda)$ that compares the shearing frequency ω to the turbulence relaxation time scale Λ.

The $\Lambda(t)$ in Eq. (23) is obtained via Eq. (13) by integrating the standard equations for $k(t)$ and $\epsilon(t)$, which for homogeneous turbulence are simply

$$\frac{dk}{dt} = P - \epsilon, \tag{24}$$

$$\frac{d\epsilon}{dt} = C_{\epsilon 1} P \frac{\epsilon}{k} - C_{\epsilon 2} \frac{\epsilon^2}{k}. \tag{25}$$

The kinetic energy production P appearing in both Eqs. (24) and (25) depends on the nonequilibrium anisotropy in Eq. (23), and is given as

$$P = -k a_{ij} \bar{S}_{ij} = -2k a_{12} \bar{S}_{12}, \tag{26}$$

where standard values of the constants are[9,12]

$$C_{\epsilon 1} = 1.44, \quad C_{\epsilon 2} = 1.83. \tag{27}$$

Alternative values of these constants are possible [for instance $C_{\epsilon 2} = 1.90$ in the LRR (Ref. 8) model], though the standard values in Eq. (27) will be used for the tests of the HD model presented herein.

Figure 2 compares the resulting anisotropy $a_{12}(t)$ from Eq. (23) with results from the LRR (Ref. 8) and SSG (Ref. 9) models, as well as with the corresponding DNS results from Yu and Girimaji[1] at shearing frequencies $\omega/S = 0.5$, 1.0, and 10. The initial nondimensional shear parameter $Sk_0/\epsilon_0 = 3.3$ was used for all simulations,[1] where k_0 and ϵ_0 are the initial turbulence kinetic energy and dissipation rate, respectively. The analytical result in Eq. (23) from the HD model in Eq. (20) shows remarkably good agreement with the DNS results. For all shearing frequencies, the amplitude and phase agreement with the DNS results is good, and for the $\omega/S = 10$ case the amplitude of the anisotropy variations shows the correct large reduction. The effect of the initial transient can be clearly distinguished in the $\omega/S = 0.5$ and $\omega/S = 1.0$ cases, where it takes approximately a full shearing cycle before the anisotropy variation becomes centered on zero with constant amplitude.

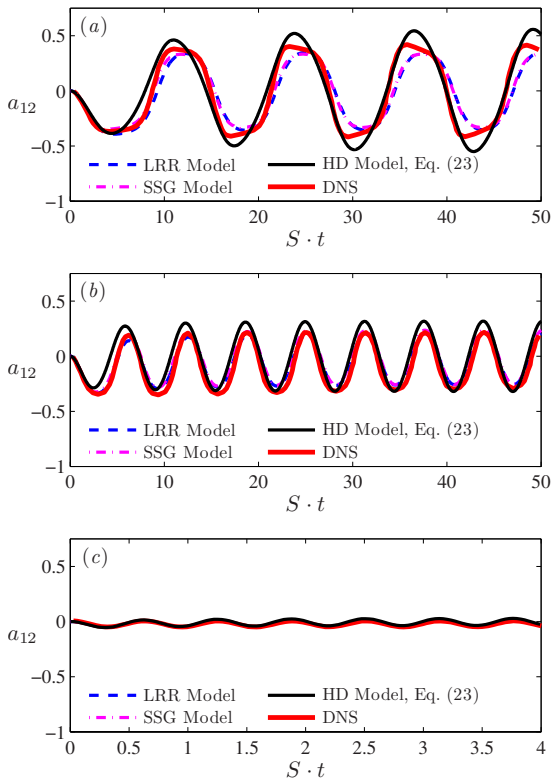

FIG. 2. (Color online) Anisotropy $a_{12}(t)$ in periodically sheared turbulence for relative shearing frequencies $\omega/S = 0.5$ (a), 1.0 (b), and 10 (c), comparing the present solution in Eq. (23) with results from the LRR (Ref. 8) and SSG (Ref. 9) models and with corresponding DNS results of Yu and Girimaji (Ref. 1).

For $\omega/S = 0.5$ in Fig. 2(a), at large times the LRR and SSG models show significantly poorer phase agreement with the DNS results than does the present analytical result in Eq. (23), despite giving slightly better prediction of the anisotropy amplitude at this frequency. For the two higher shearing frequencies in Figs. 2(b) and 2(c), the phase and amplitude from the LRR and SSG models are only slightly better than those from Eq. (23), and all are in generally good agreement with the DNS results. The result in Eq. (23), which was obtained via Eq. (20) from the quasilinear anisotropy dynamics in Eq. (12), thus retains the most relevant dynamics governing the evolution of the anisotropy in periodically sheared turbulence, giving results for the shear anisotropy that are of nearly comparable fidelity as the more computationally intensive LRR and SSG models. Moreover, the solution in Eq.

Downloaded 29 May 2009 to 141.24.81.5. Redistribution subject to AIP license or copyright; see http://pof.aip.org/pof/copyright.jsp

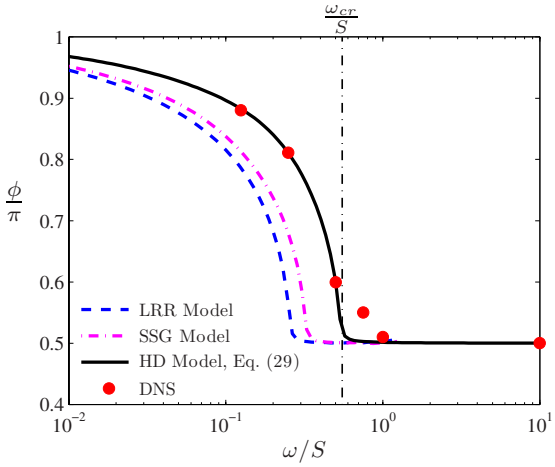

FIG. 3. (Color online) Phase difference between the shear stress anisotropy and the applied mean shear, showing good agreement of the present result in Eq. (29) with the DNS results of Yu and Girimaji (Ref. 1), and comparisons with corresponding LRR (Ref. 8) and SSG (Ref. 9) model results.

(23) allows simple analytical scalings to be identified for various key dynamical quantities in the full equilibrium limit and the quasiequilibrium and saturated nonequilibrium regimes.

D. Anisotropy phase response

In the long-time limit, after initial transients have sufficiently decayed and thus $e^{-t/\Lambda}\to 0$, the anisotropy in Eq. (23) can be written as

$$a_{12}(t) = -C_\mu \alpha_1 \left(\frac{S}{\omega}\right)\left[\frac{\omega\Lambda}{1+(\omega\Lambda)^2}\right][\sin(\omega t) - (\omega\Lambda)\cos(\omega t)]. \tag{28}$$

Defining the phase difference ϕ as the lag between the zero-crossing times for the anisotropy $a_{12}(t)$ and the applied shear $\bar{S}_{12}(t)$ in the long-time limit $S\cdot t\to\infty$, this phase lag can be obtained analytically from Eq. (28) as

$$\phi = \pi - \tan^{-1}[\omega\Lambda(t_0)], \tag{29}$$

where t_0 denotes the time at which $a_{12}=0$.

Figure 3 shows that the analytical result for ϕ in Eq. (29) agrees well with the DNS results of Yu and Girimaji[1] over a wide range of shearing frequencies ω/S. For small values of ω/S, corresponding to the quasiequilibrium regime, the phase difference approaches π in the full equilibrium limit $\omega/S\to 0$, where $a_{12}(t)$ responds instantly to changes in $\bar{S}_{12}(t)$. As ω/S increases, nonequilibrium effects become significant and ϕ smoothly approaches $\pi/2$, as shown in Fig. 3. For values of ω above a critical frequency ω_{cr}, the dynamics reach a saturated nonequilibrium regime for which the phase difference remains at the frequency-independent value $\pi/2$. From Fig. 3 it is apparent that $\omega_{cr}/S\approx 0.5$, although a more precise value will be obtained analytically in Sec. III B.

Figure 3 also shows that in contrast to the present analytical result in Eq. (29), the phase responses from the LRR and SSG second-moment models agree more poorly with the DNS results. In particular, both models significantly underpredict the critical frequency ω_{cr}, in agreement with Fig. 31 of Yu and Girimaji,[1] leading to poorer phase agreement with the DNS results for $\omega<\omega_{cr}$. This in turn is the origin of the slight phase errors from the standard LRR and SSG models for $\omega/S=0.5$ in Fig. 2(a). While both the LRR and SSG results might be improved by changing the model constants in Eqs. (10) and (11), for periodically sheared homogeneous turbulence Fig. 3 shows that the standard values of these constants do not give results for the phase response at $\omega<\omega_{cr}$ that are as accurate as the result in Eq. (29) from the solution in Eq. (23) to the HD model in Eq. (20). Yu and Girimaji[1] noted that accurate prediction of the "slow" contribution to the pressure-strain correlation Π_{ij} is critical for correctly capturing the dynamics of periodically sheared turbulence, and thus improvements to the LRR and SSG models might be achievable through a reexamination of the C_1 and C_5 terms in Eq. (6).

Before continuing, it should be noted that in Fig. 3 the transition to $\phi=\pi/2$ in the saturated nonequilibrium regime in the LRR and SSG models, and in the HD model is remarkably abrupt. The same abrupt transition is also observed, although to a lesser extent, in the DNS results (however, see Sec. III B). This is indicative of a bifurcation in the turbulence dynamics at the critical frequency ω_{cr}. The result in Eq. (29) suggests that the observed $\phi=\pi/2$ for all $\omega>\omega_{cr}$ is a result of $(\omega\Lambda)\to\infty$ above the critical frequency. This in turn suggests that $\Lambda\to\infty$ in the long-time limit $S\cdot t\to\infty$, while for $\omega<\omega_{cr}$ the associated Λ remains finite for all time. The long-time limit of Λ for $\omega>\omega_{cr}$ will be explored in more detail in Sec. IV, and it will be shown in Sec. III that ω_{cr} has a value that is determined by the model constants in Eqs. (23)–(25).

E. Anisotropy limit forms

From a physical standpoint, the parameter $(\omega\Lambda)$ characterizes how rapidly the applied shear varies with respect to the turbulence relaxation time scale Λ, and is thus the appropriate nonequilibrium parameter for periodically sheared turbulence. However, Λ is itself part of the turbulence response to the applied shearing, and for this reason ω/S provides an alternative nonequilibrium parameter that involves only variables associated with the applied periodic shear. It will be seen later herein that the cycle average of $(\omega\Lambda)$ increases monotonically with ω/S, and thus either can be used as a nonequilibrium parameter. In this section we consider the characteristics of the turbulence anisotropy in the full equilibrium limit $\omega/S\to 0$ where $(\omega\Lambda)\to 0$, in the quasiequilibrium regime for small ω/S where $(\omega\Lambda)\ll 1$, and in the saturated nonequilibrium regime where $(\omega\Lambda)\to\infty$ for all $\omega>\omega_{cr}$.

For $\omega/S\to 0$ and $(\omega\Lambda)\to 0$, the turbulence responds more rapidly than the variations in the applied shear, allowing the turbulence anisotropy to remain in full equilibrium with the mean shear. Thus the resulting anisotropy in the long-time limit from Eq. (28) is

Downloaded 29 May 2009 to 141.24.81.5. Redistribution subject to AIP license or copyright; see http://pof.aip.org/pof/copyright.jsp

$$\lim_{(\omega\Lambda)\to 0} a_{12}(t) = -C_\mu \frac{Sk}{\epsilon}\sin(\omega t), \tag{30}$$

which from Eq. (3) is identical to the result from the classical equilibrium Boussinesq closure in Eq. (18), where the anisotropy is assumed to be directly proportional to the instantaneous mean strain rate. The full equilibrium result in Eq. (30) for the anisotropy is consistent with the phase results in Fig. 3, where the phase difference between the anisotropy and the shear approaches $\phi=\pi$ for small ω/S, and hence small $(\omega\Lambda)$. However, it can be seen from Eq. (29) in Fig. 3 that even for shearing frequencies as small as $\omega/S=0.01$, the turbulence is still not fully in equilibrium with the applied shear. This result establishes the existence of a quasiequilibrium regime for small but nonzero values of ω/S corresponding to $(\omega\Lambda)\ll 1$, where the anisotropy is given as

$$\lim_{(\omega\Lambda)\ll 1} a_{12}(t) = -C_\mu \frac{Sk}{\epsilon}[\sin(\omega t) - (\omega\Lambda)\cos(\omega t)]. \tag{31}$$

The full equilibrium result in Eq. (30) for $(\omega\Lambda)\to 0$ is only obtained as $\omega/S\to 0$.

In the saturated nonequilibrium regime $(\omega\Lambda)\to\infty$, the turbulence response is far slower than the rate at which the mean shear varies. In this regime, the anisotropy from Eq. (28) is thus

$$\lim_{(\omega\Lambda)\to\infty} a_{12}(t) = C_\mu \alpha_1 \left(\frac{S}{\omega}\right)\cos(\omega t). \tag{32}$$

It is apparent in Eq. (32) that the amplitude of the anisotropy decreases with increasing shearing frequency as ω^{-1}, and that the phase difference relative to $\bar{S}_{12}(t)$ in Eq. (3) is constant at $\phi=\pi/2$, independent of Λ or ω. The abrupt switch to $\phi=\pi/2$ at $\omega=\omega_{cr}$ in Fig. 3 suggests that Eq. (32) describes the anisotropy for all $\omega>\omega_{cr}$.

The root mean square (rms) amplitude of the anisotropy gives additional insights into the turbulence response in the full equilibrium limit and the saturated nonequilibrium regime, and also into the abrupt transition in the dynamics at ω_{cr}. We define

$$\langle f\rangle \equiv \lim_{t\to\infty} \frac{\omega}{2\pi}\int_{t-\pi/\omega}^{t+\pi/\omega} f(t')dt', \tag{33}$$

as the long-time cycle average of any time-dependent quantity $f(t)$, and note that the rms amplitude of the anisotropy, here denoted a'_{12}, is defined as $(a'_{12})^2 \equiv \langle a_{12}^2\rangle - \langle a_{12}\rangle^2$. From Eq. (28), it is apparent that in the long-time limit $\langle a_{12}\rangle = 0$ for all shearing frequencies, giving

$$\lim_{(\omega\Lambda)\to 0} a'_{12} = C_\mu \alpha_1 S \langle \Lambda^2 \sin^2(\omega t)\rangle^{1/2}, \tag{34}$$

in the full equilibrium limit. It will be seen in Secs. III and IV that the existence of a fixed point in the dynamics of $\langle\Lambda\rangle$ for $\omega<\omega_{cr}$ yields the relation

$$\lim_{(\omega\Lambda)\to 0} \langle \Lambda^2 \sin^2(\omega t)\rangle = \frac{1}{C_\mu \alpha_1^2 S^2}\left[\frac{C_{\epsilon 2}-1}{C_{\epsilon 1}-1}\right], \tag{35}$$

which allows Eq. (34) to be written as

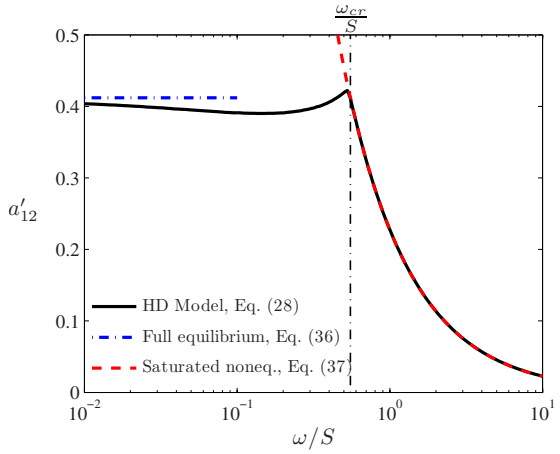

FIG. 4. (Color online) rms amplitude of the long-time limit anisotropy from Eq. (28), showing approach to equilibrium limit value in Eq. (36) and good agreement with the form for the saturated nonequilibrium regime in Eq. (37) for $\omega>\omega_{cr}$.

$$\lim_{(\omega\Lambda)\to 0} a'_{12} = \left[\frac{C_\mu(C_{\epsilon 2}-1)}{C_{\epsilon 1}-1}\right]^{1/2} = 0.41, \tag{36}$$

where values of the constants in Eqs. (21) and (27) have been used to obtain the numerical result. The corresponding form of a'_{12} in the saturated nonequilibrium regime where $(\omega\Lambda)\to\infty$ is given by

$$\lim_{(\omega\Lambda)\to\infty} a'_{12} = \frac{C_\mu \alpha_1}{\sqrt{2}}\left(\frac{S}{\omega}\right). \tag{37}$$

Figure 4 shows the resulting frequency dependence of a'_{12} obtained from the long-time limit anisotropy in Eq. (28), and also shows the equilibrium and nonequilibrium limit forms given by Eqs. (36) and (37), respectively. For small ω/S, a'_{12} approaches the full equilibrium result in Eq. (36), but even for $\omega/S=0.01$ it is clear that the turbulence is not fully in equilibrium with the applied shear, consistent with the phase results in Fig. 3. For all $\omega>\omega_{cr}$, a'_{12} decreases as $(\omega/S)^{-1}$ in accordance with the saturated nonequilibrium result in Eq. (37). As with the phase results in Fig. 3, Fig. 4 shows that a'_{12} transitions abruptly at ω_{cr} to the nonequilibrium form in Eq. (37), again reflecting the fact that $(\omega\Lambda)\to\infty$ in the saturated nonequilibrium regime for all $\omega>\omega_{cr}$.

Figures 3 and 4 thus indicate that the full equilibrium limit of periodically sheared turbulence is attained only at very small shearing frequencies as $\omega/S\to 0$. At slightly larger frequencies, the turbulence is in a quasiequilibrium regime where $(\omega\Lambda)\ll 1$. As ω/S continues to increase, but remains below ω_{cr}/S, the degree of nonequilibrium increases smoothly, as indicated by the gradual approach of the phase difference ϕ to $\pi/2$ in Fig. 3. At the critical frequency ω_{cr}, however, the turbulence abruptly transitions to the saturated nonequilibrium regime, where the phase difference remains constant at $\pi/2$ and the anisotropy amplitude begins to decrease as ω^{-1}. It can be inferred from the abrupt transition at ω_{cr} to the saturated nonequilibrium regime that $(\omega\Lambda)\to\infty$ in the long-time limit for all $\omega>\omega_{cr}$. This result will be explored in more detail in Secs. III and IV.

Downloaded 29 May 2009 to 141.24.81.5. Redistribution subject to AIP license or copyright; see http://pof.aip.org/pof/copyright.jsp

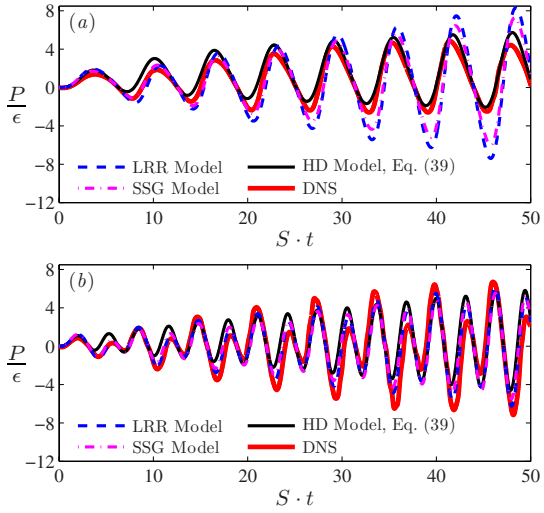

FIG. 5. (Color online) Time-evolution of the production-to-dissipation ratio P/ϵ from Eq. (39) for frequencies $\omega/S=0.5$ (a) and 1.0 (b), showing good agreement with DNS results of Yu and Girimaji (Ref. 1).

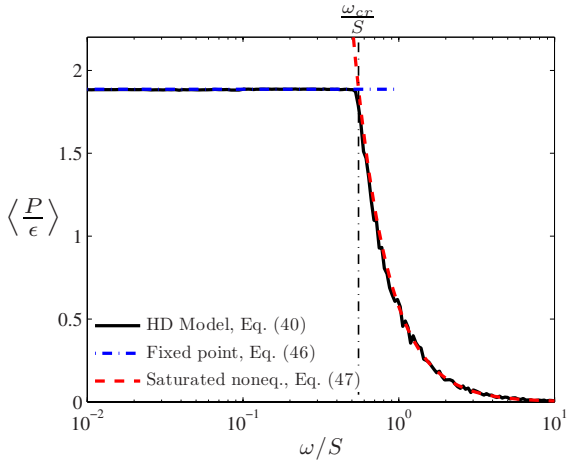

FIG. 6. (Color online) Cycle average of P/ϵ in long-time limit from Eq. (40), showing also fixed point form in Eq. (46) for $\omega<\omega_{cr}$, saturated nonequilibrium form in Eq. (47) for $\omega>\omega_{cr}$, and abrupt transition at the critical frequency ω_{cr} given in Eqs. (48) and (49).

III. PRODUCTION-TO-DISSIPATION RATIO

From Eq. (26), the production-to-dissipation ratio P/ϵ is

$$\frac{P}{\epsilon}=-\frac{k}{\epsilon}a_{ij}\bar{S}_{ij}, \tag{38}$$

and thus in periodically sheared turbulence from Eq. (23), this becomes

$$\frac{P}{\epsilon}=C_\mu\alpha_1^2\left(\frac{S}{\omega}\right)^2\left[\frac{(\omega\Lambda)^2}{1+(\omega\Lambda)^2}\right]\times\{\sin^2(\omega t)-(\omega\Lambda)\sin(\omega t)[\cos(\omega t)-e^{-t/\Lambda}]\}. \tag{39}$$

The resulting evolution of P/ϵ from Eq. (39) is shown for shearing frequencies $\omega/S=0.5$ in Fig. 5(a) and for $\omega/S=1.0$ in Fig. 5(b). The evolution of P/ϵ in Eq. (39) can be seen in Fig. 5 to agree better with the DNS results in many respects than do the results from the second-order RANS models, although the asymmetry at the higher frequency is not captured. The characteristic frequency of P/ϵ from Eq. (39) is correctly seen to be twice that of the applied shear. This latter result can be understood in the long-time limit $S\cdot t\to\infty$, where initial transients have fully decayed, which from Eq. (39) then gives

$$\frac{P}{\epsilon}=\frac{C_\mu\alpha_1^2}{2}\left(\frac{S}{\omega}\right)^2\left[\frac{(\omega\Lambda)^2}{1+(\omega\Lambda)^2}\right][1-\cos(2\omega t)-(\omega\Lambda)\sin(2\omega t)], \tag{40}$$

where the frequency doubling can be seen explicitly.

A. Production-to-dissipation limit forms

In the long-time full equilibrium limit where $(\omega\Lambda)\to 0$, with Λ from Eq. (13), the production-to-dissipation ratio from Eq. (40) becomes

$$\lim_{(\omega\Lambda)\to 0}\frac{P}{\epsilon}=C_\mu\left(\frac{Sk}{\epsilon}\right)^2\sin^2(\omega t). \tag{41}$$

As with the anisotropy $a_{12}(t)$ in the full equilibrium limit in Eq. (30), this form, which is valid for $\omega/S\to 0$, is identical to the result that would be obtained from the equilibrium Boussinesq closure. In the quasiequilibrium regime for small but nonzero ω/S, where $(\omega\Lambda)\ll 1$, P/ϵ is given by

$$\lim_{(\omega\Lambda)\ll 1}\frac{P}{\epsilon}=C_\mu\left(\frac{Sk}{\epsilon}\right)^2\left[\sin^2(\omega t)-\frac{(\omega\Lambda)}{2}\sin(2\omega t)\right]. \tag{42}$$

In the saturated nonequilibrium regime where $(\omega\Lambda)\to\infty$ for all $\omega>\omega_{cr}$, P/ϵ from Eq. (40) becomes

$$\lim_{(\omega\Lambda)\to\infty}\frac{P}{\epsilon}=\frac{C_\mu\alpha_1^2}{2}\left(\frac{S}{\omega}\right)^2[1-\cos(2\omega t)-(\omega\Lambda)\sin(2\omega t)], \tag{43}$$

and since $(\omega\Lambda)$ is large in this limit, the amplitude of the P/ϵ fluctuations becomes correspondingly large.

While Eqs. (41)–(43) provide insights into the time dynamics of P/ϵ in the full equilibrium limit and the quasiequilibrium and saturated nonequilibrium regimes, it is the cycle average value of P/ϵ that determines the asymptotic behavior of the turbulence kinetic energy k and the relaxation time scale Λ. Applying the definition of the cycle average from Eq. (33) to Eq. (40) gives the resulting frequency response of $\langle P/\epsilon\rangle$ shown in Fig. 6, where frequency-independent scaling is observed for $\omega<\omega_{cr}$, and power-law scaling is observed in the saturated nonequilibrium regime for $\omega>\omega_{cr}$.

The low- and high-frequency scaling of $\langle P/\epsilon\rangle$ in Fig. 6 can be understood analytically from the long-time limit forms of $\langle P/\epsilon\rangle$ obtained from Eq. (40). In the full equilibrium limit $(\omega\Lambda)\to 0$, the cycle average of Eq. (40) is given as

Downloaded 29 May 2009 to 141.24.81.5. Redistribution subject to AIP license or copyright; see http://pof.aip.org/pof/copyright.jsp

$$\lim_{(\omega\Lambda)\to 0}\left\langle \frac{P}{\epsilon}\right\rangle = C_\mu \alpha_1^2 S^2 \langle \Lambda^2 \sin^2(\omega t)\rangle, \tag{44}$$

where there is no explicit dependence on the shearing frequency ω. While $\langle \Lambda^2 \sin^2(\omega t)\rangle$ appearing in Eq. (44) does not appear at first to permit an analytical solution, it will be seen in Sec. IV that the evolution of $\langle \Lambda\rangle$ depends on $\langle P/\epsilon\rangle$, and that there is a stable fixed point in the dynamics of $\langle \Lambda\rangle$ when

$$\left\langle \frac{P}{\epsilon}\right\rangle = \frac{C_{\epsilon 2}-1}{C_{\epsilon 1}-1}. \tag{45}$$

Equating Eqs. (44) and (45) thus provides the analytical expression for $\langle \Lambda^2 \sin^2(\omega t)\rangle$ in Eq. (35), and for the standard values of the constants in Eq. (27), Eq. (45) gives the classical value

$$\left\langle \frac{P}{\epsilon}\right\rangle = 1.89, \tag{46}$$

indicated by the horizontal dotted-dashed line in Fig. 6. The agreement between the low-frequency limit of $\langle P/\epsilon\rangle$ from Eq. (40) in Fig. 6 and the result in Eq. (46) indicates that for $\omega < \omega_{cr}$, the long-time dynamics of $\langle \Lambda\rangle$ correspond to the fixed point and $\langle P/\epsilon\rangle$ thus attains the frequency-independent value in Eq. (46). In the saturated nonequilibrium regime $\omega > \omega_{cr}$ where $(\omega\Lambda)\to\infty$ and $\langle \Lambda \sin(2\omega t)\rangle$ is negligible, the cycle average of $\langle P/\epsilon\rangle$ from Eq. (40) becomes

$$\lim_{(\omega\Lambda)\to\infty}\left\langle \frac{P}{\epsilon}\right\rangle = \frac{C_\mu \alpha_1^2}{2}\left(\frac{S}{\omega}\right)^2, \tag{47}$$

and thus $\langle P/\epsilon\rangle$ decreases with increasing frequency as $(\omega/S)^{-2}$. The result in Eq. (47) agrees in Fig. 6 with the frequency response of $\langle P/\epsilon\rangle$ from Eq. (40) for essentially all $\omega > \omega_{cr}$.

It is the decrease in $\langle P/\epsilon\rangle$ with increasing frequency in the saturated nonequilibrium regime that is responsible for the distinctly different turbulence response for shearing frequencies above and below ω_{cr}. As the shearing frequency increases past ω_{cr}, the cycle average of $\langle P/\epsilon\rangle$ drops below the value required to support turbulence kinetic energy growth, resulting in kinetic energy decay for all $\omega > \omega_{cr}$. The asymptotic frequency response of the turbulence kinetic energy $k(t)$ and the relaxation time scale $\Lambda(t)$ is examined in more detail in Sec. IV.

B. Analytical result for the critical frequency

Due to the abrupt transition in Fig. 6 from the fixed point dynamics for $\omega < \omega_{cr}$ to the saturated nonequilibrium dynamics for $\omega > \omega_{cr}$, the corresponding limit forms of $\langle P/\epsilon\rangle$ in Eqs. (45) and (47) can be used to determine an analytical result for the critical frequency ω_{cr}. Equating Eqs. (45) and (47) at $\omega = \omega_{cr}$ thus gives

$$\omega_{cr} = S\left[\frac{C_\mu (C_{\epsilon 1}-1)\alpha_1^2}{2(C_{\epsilon 2}-1)}\right]^{1/2}. \tag{48}$$

For the standard values of the constants in Eqs. (21) and (27), and α_1 in Eq. (22), the resulting critical frequency is

$$\omega_{cr} = 0.55S, \tag{49}$$

which is in good agreement with the approximate empirical value $\omega_{cr} \approx 0.5S$ reported by Yu and Girimaji[1] from their DNS results.

The fact that the critical frequency in Eq. (49) depends only on model constants may provide guidance in determining more appropriate values of the constants in Eqs. (10) and (11) for second-order closure models in unsteadily forced turbulent flows. Values for α_1 in such models can vary widely, as is evident from the fact that $\alpha_1 = 2.39$ in the LRR model and $\alpha_1 = 4.29$ in the SSG model (where again we have used the equilibrium value $P/\epsilon \approx 1.89$ to obtain α_1). In the present approach however, α_1 is dictated by ω_{cr} in Eq. (48). For the values of C_μ, $C_{\epsilon 1}$, and $C_{\epsilon 2}$ in Eqs. (21) and (27) we *must* have $\alpha_1 \approx 3.57$ in order to have $\omega_{cr} \approx 0.5S$ as observed in the DNS data.

With respect to the DNS study by Yu and Girimaji,[1] Fig. 3 shows that the critical frequency ω_{cr} is more clearly defined in the HD model[10] than in the DNS results, thereby allowing the precise determination of ω_{cr} in Eq. (49). Whereas the HD model transitions abruptly to the saturated nonequilibrium regime at ω_{cr}, the DNS results indicate a more gradual approach to this regime. The slight differences between the HD model and DNS results near ω_{cr} are most likely due, in part, to the physical approximations used in the formulation of the HD model. At the same time however, owing to the substantial computational demands of the DNS approach used in the Yu and Girimaji[1] study, a precise determination of the critical frequency such as that provided in Eq. (49) was impractical. Only a limited number of frequencies could be simulated, as evident in Fig. 3, and—even more importantly—for $\omega \approx \omega_{cr}$ the simulations would need to have run for impractically long times to accurately discern between the extremely slow average rates of growth and decay in the otherwise oscillatory $k(t)$ as ω_{cr} is crossed. Similarly, it will be seen in Sec. IV that as ω_{cr} is crossed, $\langle \Lambda\rangle$ grows only very slowly with increasing time t, thus requiring simulation times much greater than $S\cdot t = 50$ in order to obtain $\langle \Lambda\rangle \to \infty$ and the corresponding asymptotic phase shift $\phi = \pi/2$ from Eq. (29). It is thus likely that the small differences between the HD model and DNS results near ω_{cr} are due to a combination of effects from the physical simplifications used to derive the HD model, as well as the practical limitations of the DNS.

IV. TURBULENCE KINETIC ENERGY AND RELAXATION TIME

The turbulence kinetic energy $k(t)$ is determined by Eqs. (24)–(26), with $\bar{S}_{12}(t)$ from Eq. (3) and $a_{12}(t)$ from Eq. (23). Results are shown for a range of shearing frequencies ω/S in Fig. 7. It can be seen that the kinetic energy varies with a frequency twice that of the applied shear, consistent with the frequency doubling seen in Eq. (40). Its cycle average value $\langle k\rangle$ can be seen in Fig. 7 to grow for frequencies below the $\omega_{cr}/S = 0.55$ critical value, and decay for higher frequencies, in agreement with the findings of Yu and Girimaji.[1] As noted

Downloaded 29 May 2009 to 141.24.81.5. Redistribution subject to AIP license or copyright; see http://pof.aip.org/pof/copyright.jsp

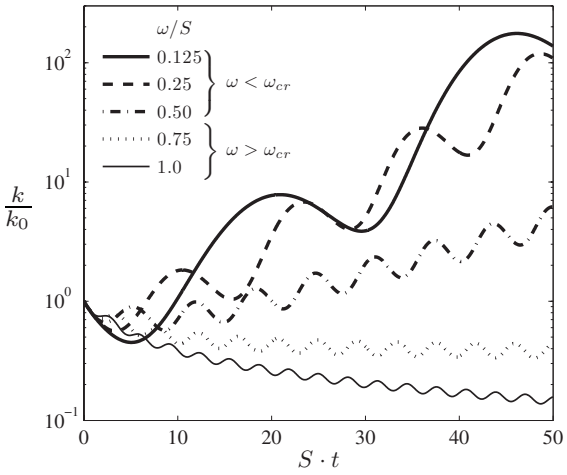

FIG. 7. Kinetic energy evolution $k(t)$ normalized by the initial value k_0 for various shearing frequencies ω/S, showing the transition from kinetic energy growth ($\omega < \omega_{cr}$) to decay ($\omega > \omega_{cr}$) at the critical frequency $\omega_{cr}/S = 0.55$ from Eq. (48).

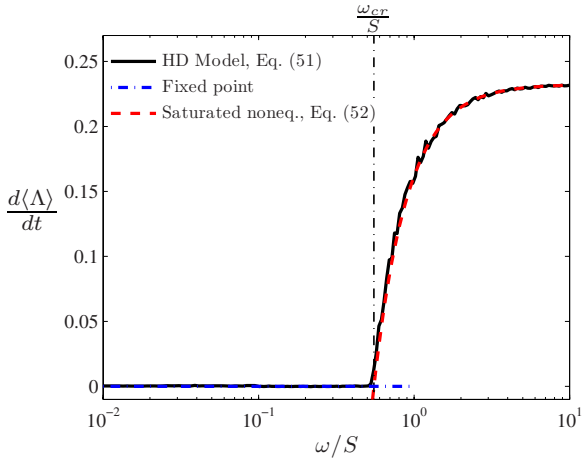

FIG. 9. (Color online) Frequency response of $d\langle\Lambda\rangle/dt$ in long-time limit from Eq. (51), showing fixed point dynamics for $\omega < \omega_{cr}$ and good agreement with saturated nonequilibrium form in Eq. (52) for $\omega > \omega_{cr}$.

in Sec. III A, the decay in $k(t)$ for $\omega > \omega_{cr}$ in Fig. 7 is due to the $(\omega/S)^{-2}$ decrease in the cycle average of P/ϵ in the saturated nonequilibrium regime.

From Eqs. (24) and (25), the dynamical equation for the turbulence relaxation time scale $\Lambda(t)$ is

$$\frac{d\Lambda}{dt} = \frac{1}{\alpha_1}(1 - C_{\epsilon 1})\frac{P}{\epsilon} + \frac{1}{\alpha_1}(C_{\epsilon 2} - 1). \tag{50}$$

Figure 8 shows the evolution of $\Lambda(t)$ for various shearing frequencies, where the transition in the dynamics is apparent as the frequency increases past ω_{cr}. The cycle average value $\langle\Lambda\rangle$ grows without bound for $\omega > \omega_{cr}$, while for $\omega < \omega_{cr}$ the resulting $\Lambda(t)$ oscillates around a mean that remains constant after the initial transient has decayed.

As with the production-to-dissipation ratio in Sec. III B, the cycle average $\langle\Lambda\rangle$ reveals the transition in the dynamics as ω increases above the critical value ω_{cr}. From the equation for Λ in Eq. (50), the corresponding equation for $\langle\Lambda\rangle$ is

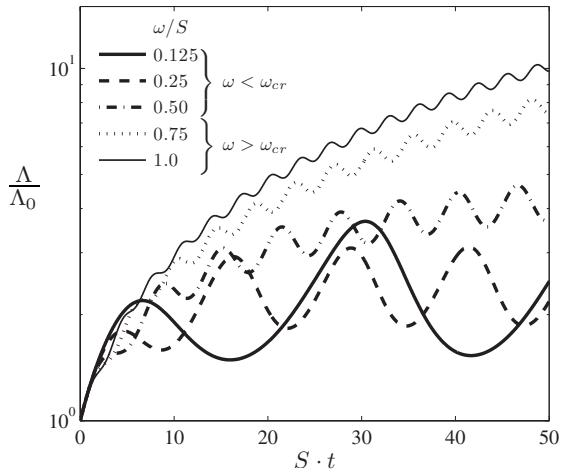

FIG. 8. Evolution of the turbulence relaxation time scale Λ normalized by the initial value Λ_0 for various shearing frequencies ω/S. The magnitude of Λ becomes unbounded in the long-time limit for shearing frequencies above the critical value $\omega_{cr}/S = 0.55$.

$$\frac{d\langle\Lambda\rangle}{dt} = \frac{1}{\alpha_1}(1 - C_{\epsilon 1})\left\langle\frac{P}{\epsilon}\right\rangle + \frac{1}{\alpha_1}(C_{\epsilon 2} - 1). \tag{51}$$

The frequency response of $d\langle\Lambda\rangle/dt$ from Eq. (51) is shown in Fig. 9, where $d\langle\Lambda\rangle/dt = 0$ for $\omega < \omega_{cr}$, and there is a clear power-law increase in $d\langle\Lambda\rangle/dt$ in the saturated nonequilibrium regime for $\omega > \omega_{cr}$.

The evolution of $\langle\Lambda\rangle$ from Eq. (51) can be understood analytically for all ω from the corresponding forms of $\langle P/\epsilon\rangle$ in Eqs. (45) and (47). For $\omega < \omega_{cr}$ there is clearly a stable fixed point in the dynamics of $\langle\Lambda\rangle$, as indicated by the fluctuations of $\Lambda(t)$ about a steady mean value for $\omega/S = 0.125$ and $\omega/S = 0.25$ in Fig. 8, and by the fact that $d\langle\Lambda\rangle/dt = 0$ for $\omega < \omega_{cr}$ in Fig. 9. In Sec. III, the existence of this fixed point was used to obtain the value of $\langle P/\epsilon\rangle$ in Eq. (45). With this, the right-hand side of Eq. (51) is thus zero, giving $\langle\Lambda\rangle$ as a time-independent value that depends on ω and S. Figure 10(a) shows $\langle\Lambda\rangle$ as a function of ω/S, where $\langle\Lambda\rangle$ generally decreases with increasing ω/S for $\omega \ll \omega_{cr}$.

In the saturated nonequilibrium regime $\omega > \omega_{cr}$, $\langle P/\epsilon\rangle$ depends on ω/S as in Eq. (47), and thus the resulting dynamical equation for $\langle\Lambda\rangle$ is

$$\lim_{(\omega\Lambda)\to\infty} \frac{d\langle\Lambda\rangle}{dt} = (1 - C_{\epsilon 1})\frac{C_\mu \alpha_1}{2}\left(\frac{S}{\omega}\right)^2 + \frac{1}{\alpha_1}(C_{\epsilon 2} - 1). \tag{52}$$

This form of $d\langle\Lambda\rangle/dt$ is seen to agree well with the result from Eq. (51) in Fig. 9 for $\omega > \omega_{cr}$, and since none of the quantities on the right-hand side vary with time, in the saturated nonequilibrium regime the cycle average $\langle\Lambda\rangle$ increases linearly with t. This results in $\langle\Lambda\rangle \to \infty$ as $S \cdot t \to \infty$ in the saturated nonequilibrium regime for all $\omega > \omega_{cr}$, as shown in Fig. 10(a).

Finally, Fig. 10(b) shows the relationship between $\langle\omega\Lambda\rangle$ and ω/S. The former is the proper nonequilibrium parameter since it compares the shearing frequency with the turbulence relaxation time, but is not known *a priori* from the specified forcing parameters ω and S for any given case. In contrast,

Downloaded 29 May 2009 to 141.24.81.5. Redistribution subject to AIP license or copyright; see http://pof.aip.org/pof/copyright.jsp

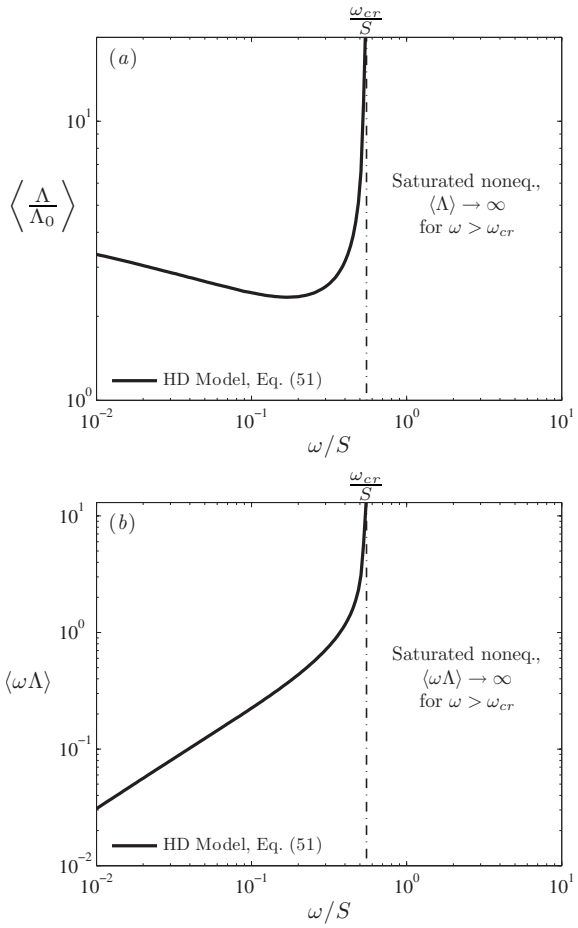

FIG. 10. Variation in the cycle average of Λ (a) and the nonequilibrium parameter $(\omega\Lambda)$ (b) in long-time limit with shearing frequency ω/S, showing $\langle\Lambda\rangle\to\infty$ and $\langle\omega\Lambda\rangle\to\infty$ for all $\omega>\omega_{\mathrm{cr}}$. (b) shows monotonic increase in $\langle\omega\Lambda\rangle$ with increasing ω/S.

ω/S can be determined directly from these parameters, and also provides an indirect indication of the degree of nonequilibrium. Figure 10(b) verifies that these two nonequilibrium parameters depend monotonically on one another, and thus either can be used to identify the extent of nonequilibrium in periodically sheared homogeneous turbulence. Consistent with the linear increase in $\langle\Lambda\rangle$ with time from Eq. (52), Fig. 10(b) shows that $\langle\omega\Lambda\rangle\to\infty$ in the saturated nonequilibrium regime for all $\omega>\omega_{\mathrm{cr}}$.

V. CONCLUSIONS

The present study has provided detailed parametric results for the dynamics of initially-isotropic homogeneous turbulence subjected to periodic shear at any shearing magnitude S and frequency ω. This flow provides insights into the effects of spatially or temporally varying shear on the anisotropy in inhomogeneous turbulent shear flows. While there have been prior DNS studies (e.g., Ref. 1) of this flow, the associated computational burden necessarily limits the number of frequencies and shearing magnitudes that can be considered. Moreover, such simulations need to be run for impractically long times to obtain a precise identification of the critical frequency ω_{cr} at which the long-time dynamics switch to the saturated nonequilibrium regime for all $\omega>\omega_{\mathrm{cr}}$. In principle, second-order closures of the RANS equations could allow a detailed parametric study of this flow, but as shown herein and in Ref. 1, the widely used standard forms of the LRR and SSG models overpredict the anisotropy phase lag and underpredict the critical frequency ω_{cr}.

The approach taken here is instead based on a quasi-analytical solution to a recently proposed nonequilibrium anisotropy closure.[10] This allows a general expression for nonequilibrium effects in the anisotropy dynamics via a convolution integral that accounts for the entire time history of the applied mean strain rate $\bar{S}_{ij}(t)$. The analytical form for $a_{ij}(t)$ was shown here to provide results for the shear anisotropy in this flow that agree well with DNS, and for some key aspects of the dynamics agree better than do the most widely used second-order moment closures. This analytical solution allows a more detailed parametric study than is practical via DNS, and provides direct insights into the parametric origins of the resulting dynamics. The long-time limit form of the shear anisotropy $a_{12}(t)$ provides an analytical expression for the resulting anisotropy phase lag. The general solution also provides simple scalings in the full equilibrium limit and the quasiequilibrium and saturated nonequilibrium regimes. In particular, the cycle average anisotropy magnitude and production-to-dissipation ratio are both essentially independent of ω for $\omega<\omega_{\mathrm{cr}}$, and in the saturated nonequilibrium regime for $\omega>\omega_{\mathrm{cr}}$ follow simple power-law scalings in (ω/S). The transition to the saturated nonequilibrium regime is shown to occur over a remarkably narrow range of ω around the critical frequency ω_{cr}, for which an analytical expression is also obtained. The fundamental change in the dynamics of the turbulence kinetic energy $k(t)$ and the turbulence relaxation time scale $\Lambda(t)$ as ω increases past ω_{cr} is also addressed. In particular, there is a fixed point regime for all $\omega<\omega_{\mathrm{cr}}$ in the dynamics of the cycle averaged Λ.

Perhaps most importantly, the present frequency response analysis indicates that at the critical frequency ω_{cr} in Eq. (48), periodically sheared homogeneous turbulence abruptly enters a saturated nonequilibrium limit that persists for all $\omega>\omega_{\mathrm{cr}}$. In particular, Fig. 10 shows that the nonequilibrium parameter $(\omega\Lambda)$ becomes unbounded as $S\cdot t\to\infty$ for all $\omega>\omega_{\mathrm{cr}}$. Moreover, for $\omega>\omega_{\mathrm{cr}}$ the anisotropy amplitude decays as ω^{-1}, the phase difference between the anisotropy and the applied shear reaches the frequency-independent value $\phi=\pi/2$, the cycle average of P/ϵ decays as ω^{-2}, and the turbulence kinetic energy k asymptotically approaches zero. This last result is in agreement with DNS,[1] and indicates that turbulence cannot be sustained for shearing frequencies greater than the critical frequency ω_{cr}.

ACKNOWLEDGMENTS

This work was supported, in part, by the Air Force Research Laboratory (AFRL) through the Michigan-AFRL Collaborative Center for Aeronautical Sciences (MACCAS) under Award No. FA8650-06-2-3625, and by the National Aeronautics and Space Administration (NASA) Marshall and Glenn Research Centers and the Department of Defense

Downloaded 29 May 2009 to 141.24.81.5. Redistribution subject to AIP license or copyright; see http://pof.aip.org/pof/copyright.jsp

(DoD) under the NASA Constellation University Institutes Project (CUIP) under Grant No. NCC3-989.

[1]D. Yu and S. S. Girimaji, "Direct numerical simulations of homogeneous turbulence subject to periodic shear," J. Fluid Mech. **566**, 117 (2006).
[2]S. S. Girimaji, J. R. O'Neill, and D. Yu, "Rapid distortion analysis of homogeneous turbulence subjected to rotating shear," Phys. Fluids **18**, 085102 (2006).
[3]D. Lohse, "Periodically kicked turbulence," Phys. Rev. E **62**, 4946 (2000).
[4]A. von der Heydt, S. Grossman, and D. Lohse, "Response maxima in modulated turbulence," Phys. Rev. E **67**, 046308 (2003).
[5]W. J. T. Bos, T. T. Clark, and R. Rubinstein, "Small scale response and modeling of periodically forced turbulence," Phys. Fluids **19**, 055107 (2007).
[6]I. Hadzic, K. Hanjalic, and D. Laurence, "Modeling the response of turbulence subjected to cyclic irrotational strain," Phys. Fluids **13**, 1739 (2001).
[7]J. Chen, C. Meneveau, and J. Katz, "Scale interactions of turbulence subjected to a straining-relaxation-destraining cycle," J. Fluid Mech. **562**, 123 (2006).
[8]B. E. Launder, G. Reece, and W. Rodi, "Progress in the development of a Reynolds stress turbulence closure," J. Fluid Mech. **68**, 537 (1975).
[9]C. G. Speziale, S. Sarkar, and T. B. Gatski, "Modeling the pressure strain correlation of turbulence: An invariant dynamical systems approach," J. Fluid Mech. **227**, 245 (1991).
[10]P. E. Hamlington and W. J. A. Dahm, "Reynolds stress closure for non-equilibrium effects in turbulent flows," Phys. Fluids **20**, 115101 (2008).
[11]S. B. Pope, *Turbulent Flows* (Cambridge University Press, Cambridge, UK, 2000).
[12]T. B. Gatski and C. G. Speziale, "On explicit algebraic stress models for complex turbulent flows," J. Fluid Mech. **254**, 59 (1993).
[13]C. G. Speziale and R. M. C. So, "Turbulence modeling and simulation," *The Handbook of Fluid Dynamics* (Springer, New York, 1998), Chap. 14, pp. 14.1–14.111.

Downloaded 29 May 2009 to 141.24.81.5. Redistribution subject to AIP license or copyright; see http://pof.aip.org/pof/copyright.jsp